Electronic Supplementary Material (ESI) for Dalton Transactions.
This journal is © The Royal Society of Chemistry 2020

ARTICLE

Electronic supplementary information

for

Red-emitting neutral rhenium(I) complexes bearing a pyridyl pyridoannelated *N*-heterocyclic carbene

Anna Bonfiglio,[a] Kevin Magra,[b] Cristina Cebrián,[b] Federico Polo,[c] Philippe C. Gros,[b,d] Pierluigi Mercandelli,[e] and Matteo Mauro*[,a]

[a] *Université de Strasbourg & CNRS, Institut de Physique et Chimie des Matériaux de Strasbourg (IPCMS), 23, rue du Loess, F-67034 Strasbourg (France), e-mail: mauro@unistra.fr*

[b] *Université de Lorraine, CNRS, L2CM, F-57000 Metz (France)*

[c] *Department of Molecular Sciences and Nanosystems, Ca' Foscari University of Venice. Via Torino 155, 30172 Venezia (Italy)*

[d] *Université de Lorraine, CNRS, L2CM, F-54000 Nancy (France)*

[e] *Dipartimento di Chimica, Università degli Studi di Milano, via Camillo Golgi 19, 20133 Milano (Italy)*

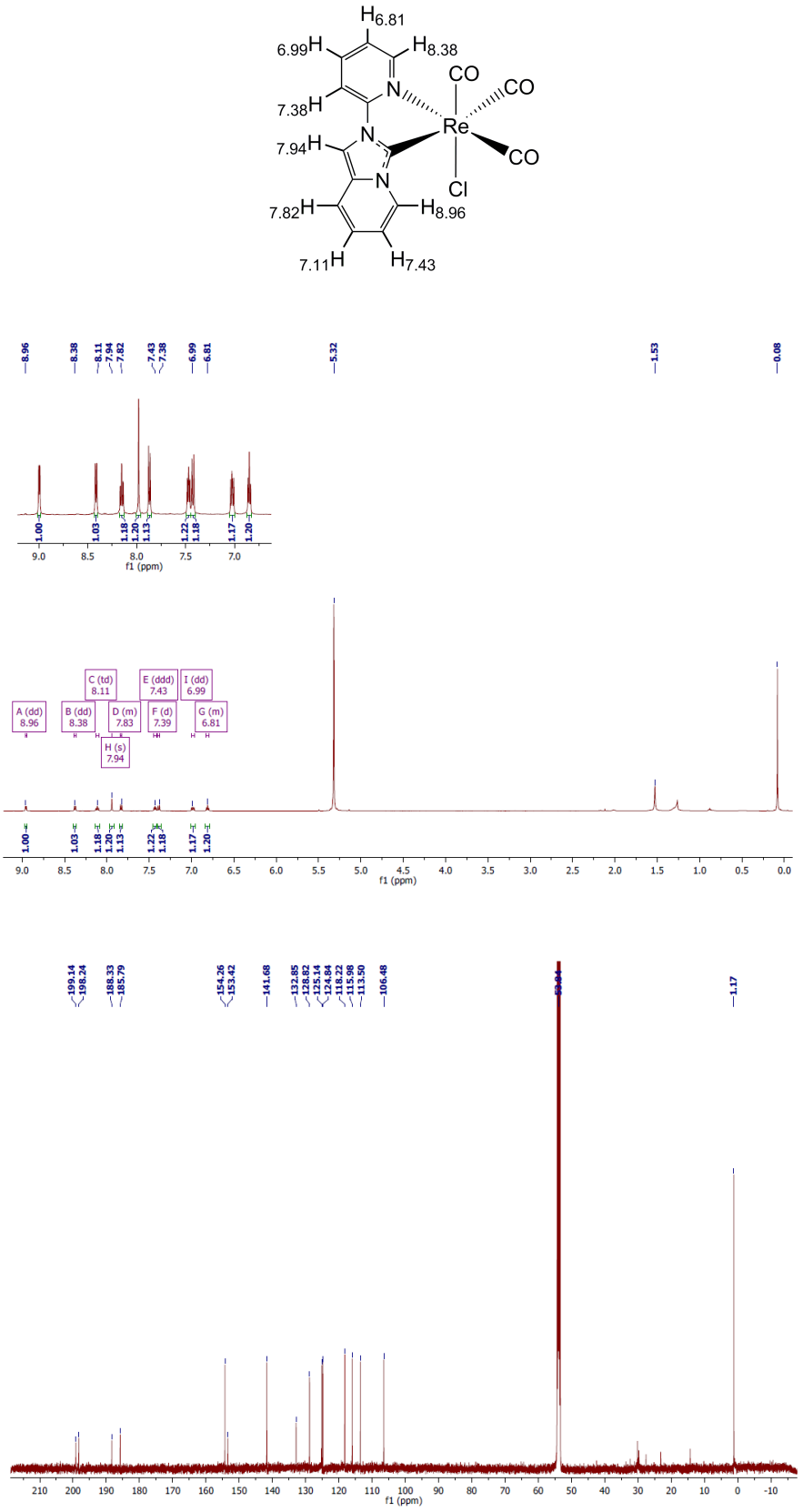

Figure S1. ^{1}H (500 MHz, *top*) and ^{13}C NMR (125 MHz, *bottom*) spectra recorded for complex **1** in CD_2Cl_2 at 298 K.

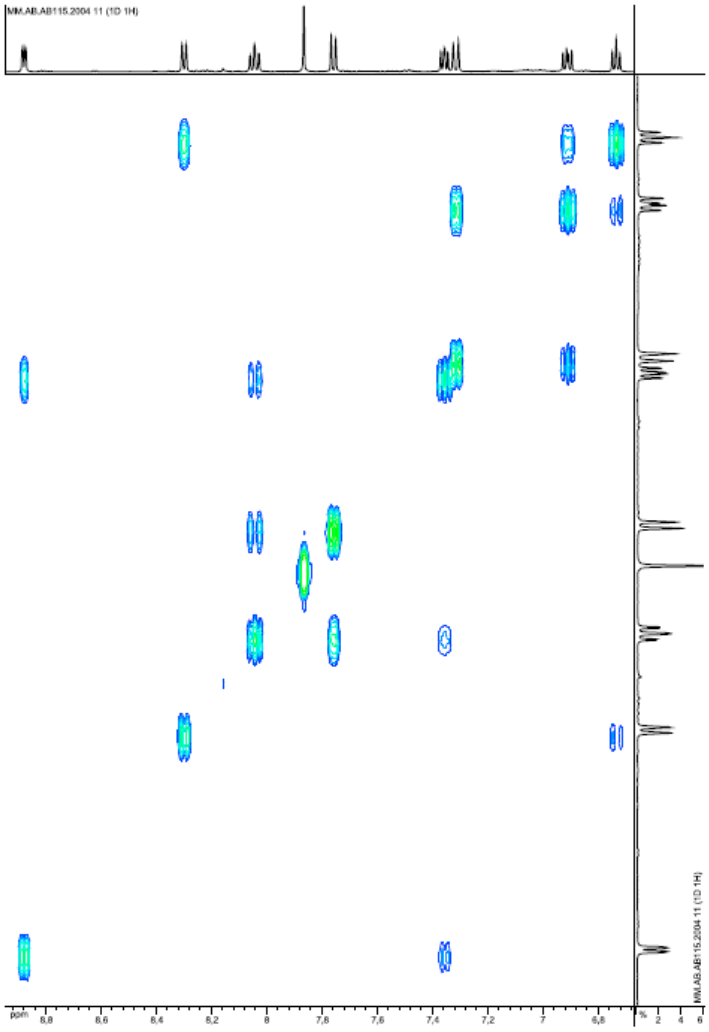

Figure S2. ^{1}H-^{1}H COSY NMR spectrum recorded for complex **1** in CD_2Cl_2 at 298 K.

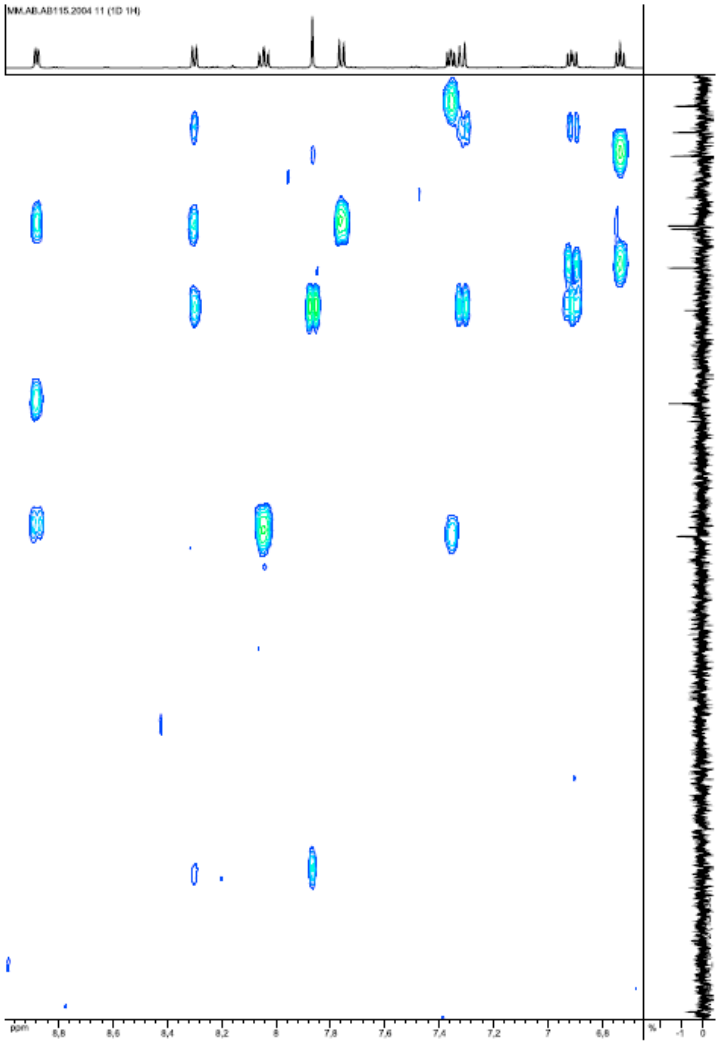

Figure S3. ^{1}H-^{13}C HMBC NMR spectrum recorded for complex **1** in CD_2Cl_2 at 298 K.

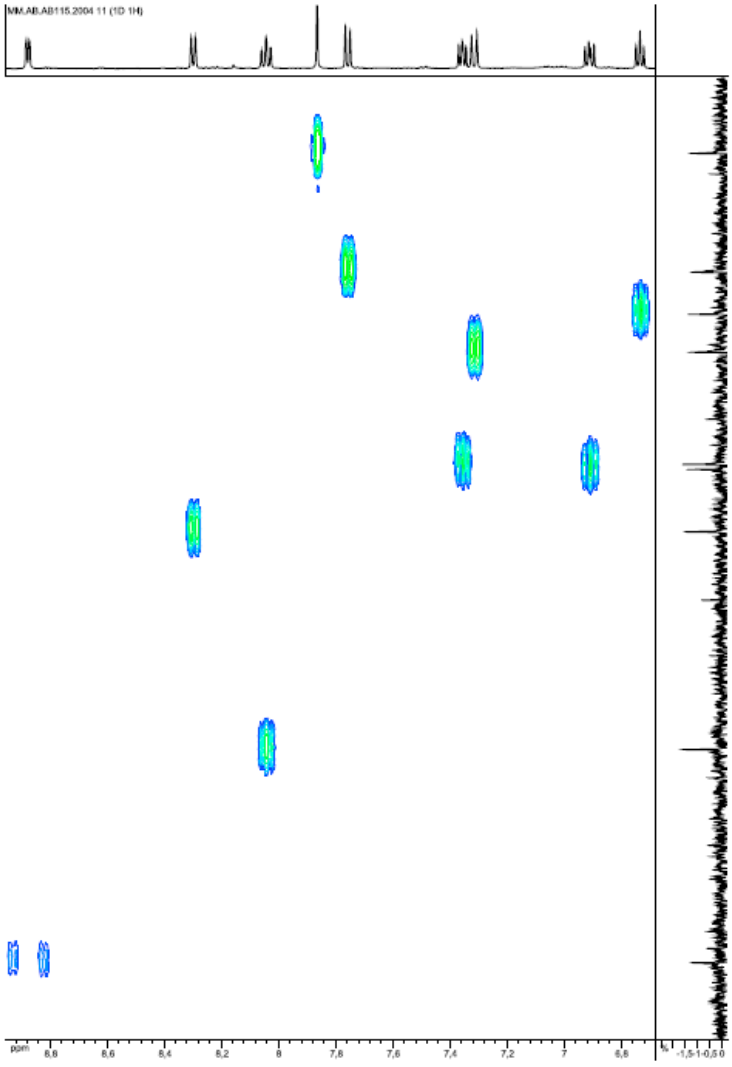

Figure S4. ^{1}H-^{13}C HSQC NMR spectrum recorded for complex **1** in CD_2Cl_2 at 298 K.

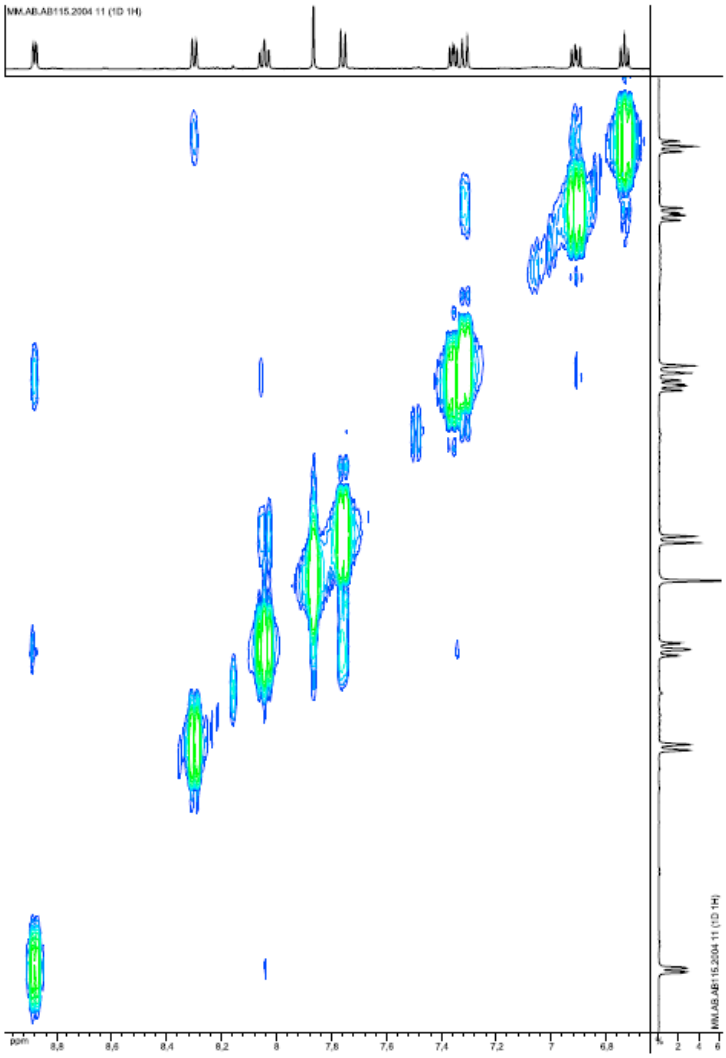

Figure S5. ^{1}H-^{1}H ROESY NMR spectrum recorded for complex **1** in CD_2Cl_2 at 298 K.

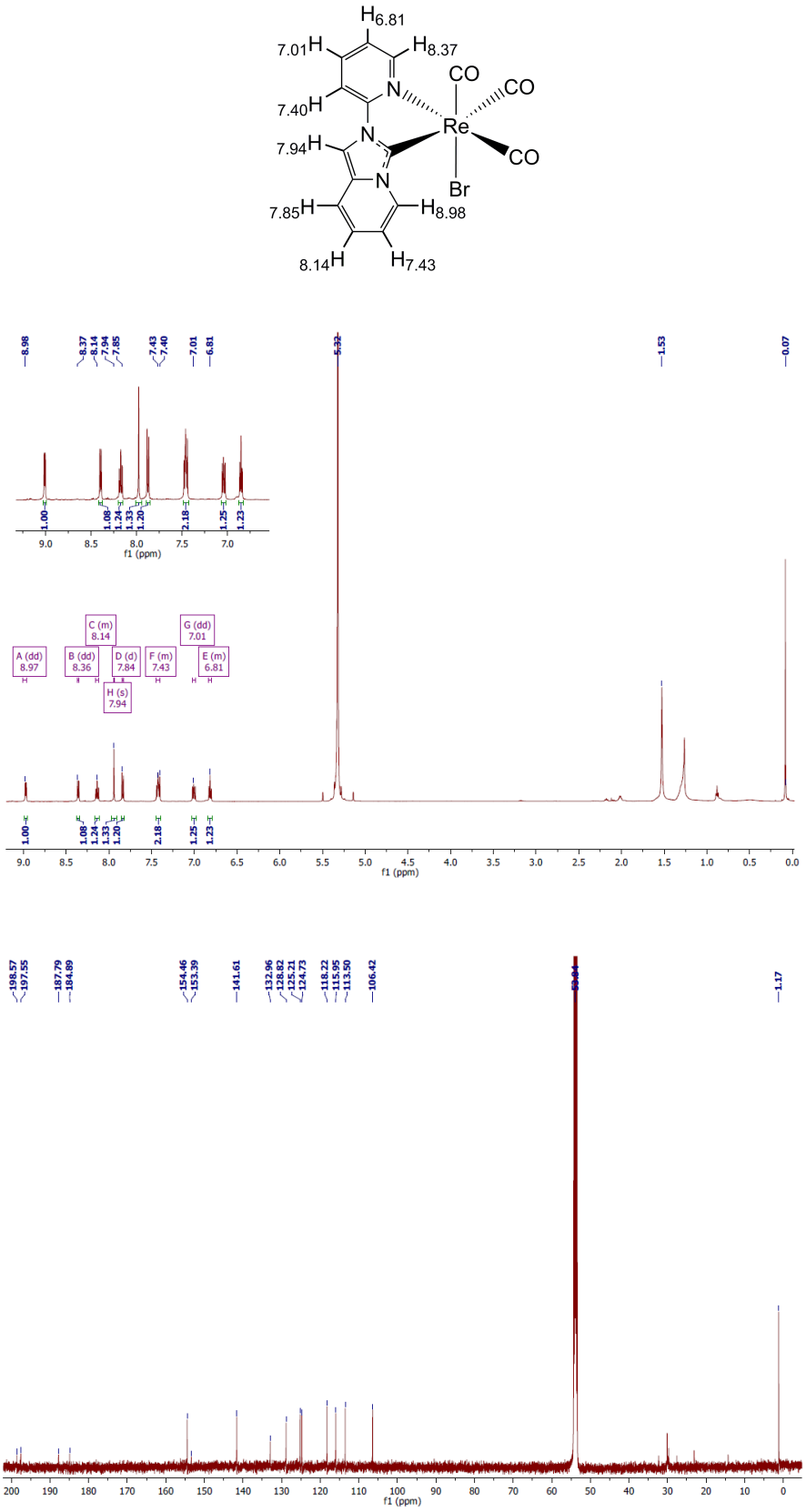

Figure S6. ^{1}H (500 MHz, *top*) and ^{13}C NMR (125 MHz, *bottom*) spectra recorded for complex **2** in CD_2Cl_2 at 298 K.

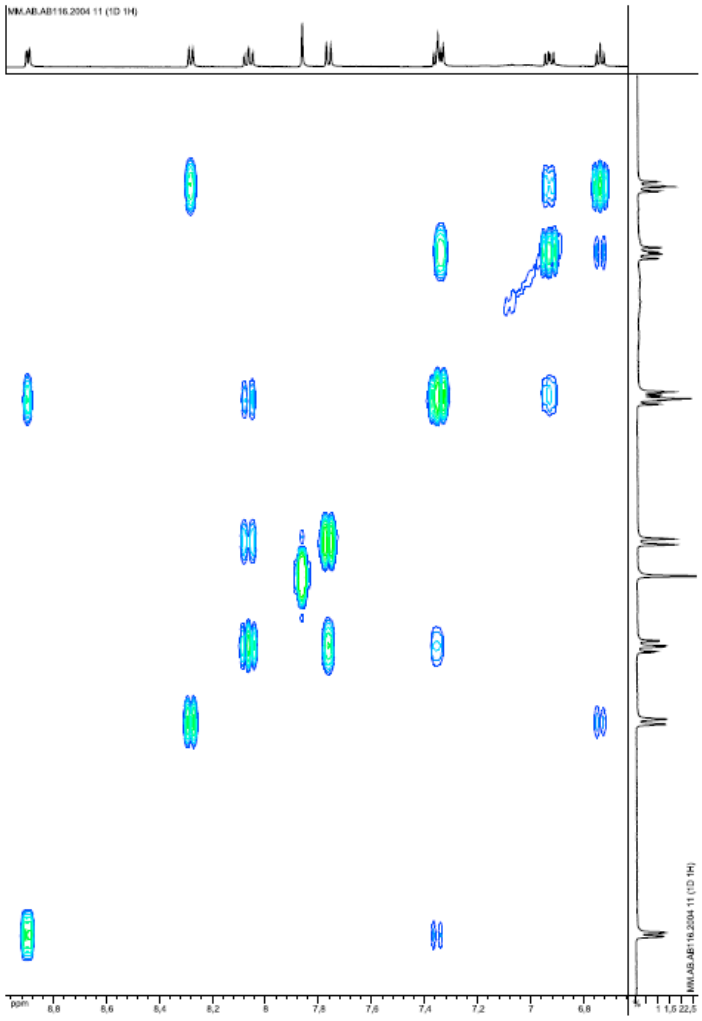

Figure S7. ^{1}H-^{1}H COSY NMR spectrum recorded for complex **2** in CD_2Cl_2 at 298 K.

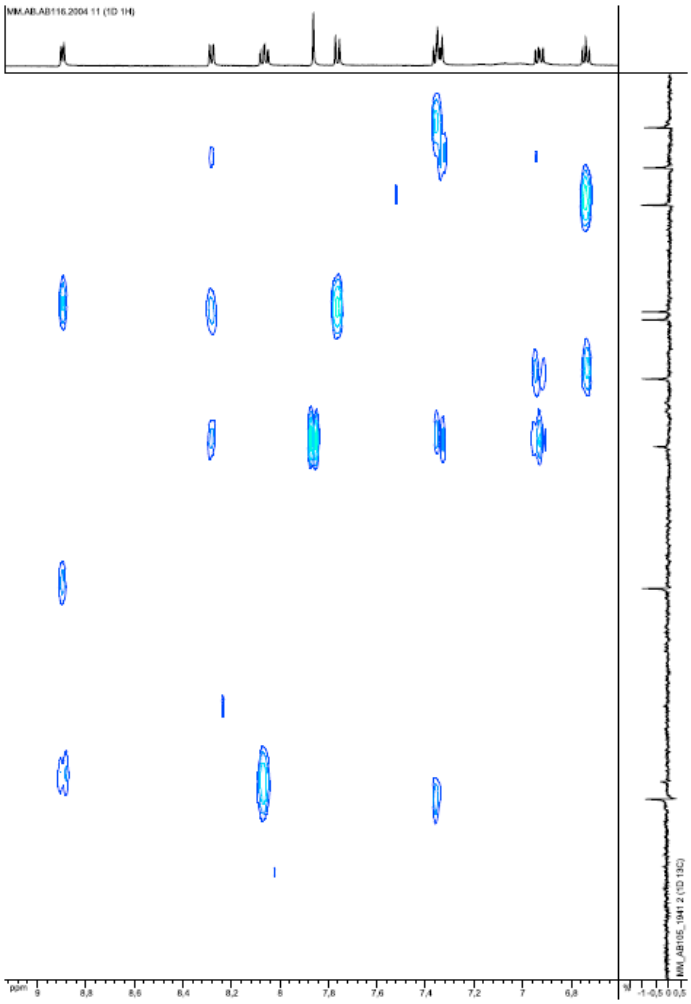

Figure S8. ^{1}H-^{13}C HMBC spectrum recorded for complex **2** in CD_2Cl_2 at 298 K.

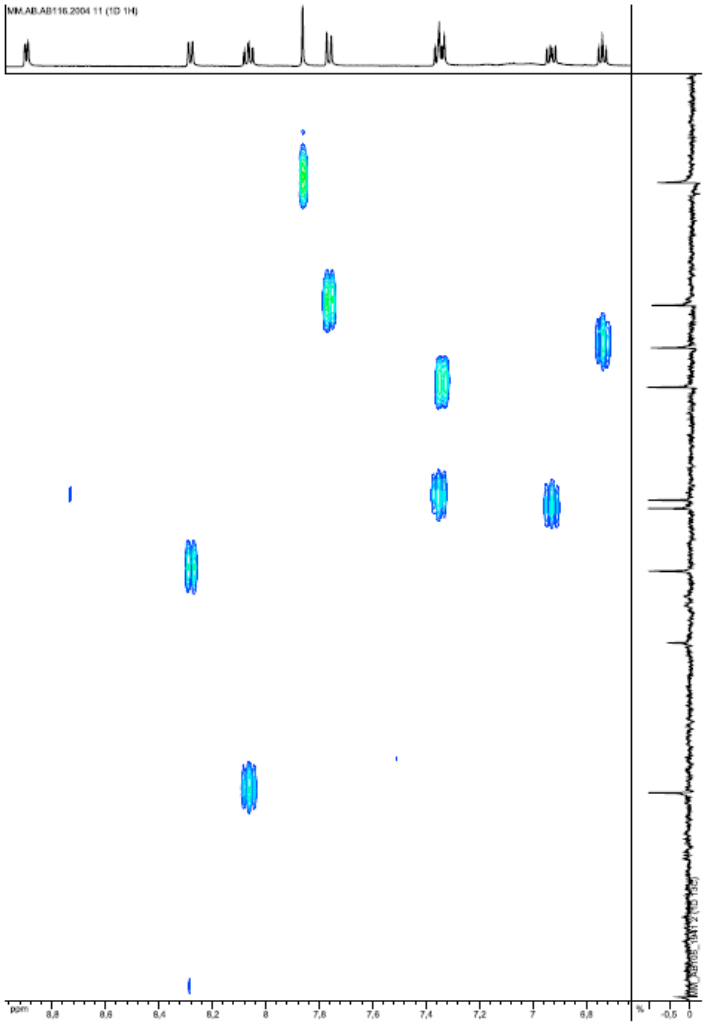

Figure S9. ^{1}H-^{13}C HSQC NMR spectrum recorded for complex **2** in CD_2Cl_2 at 298 K.

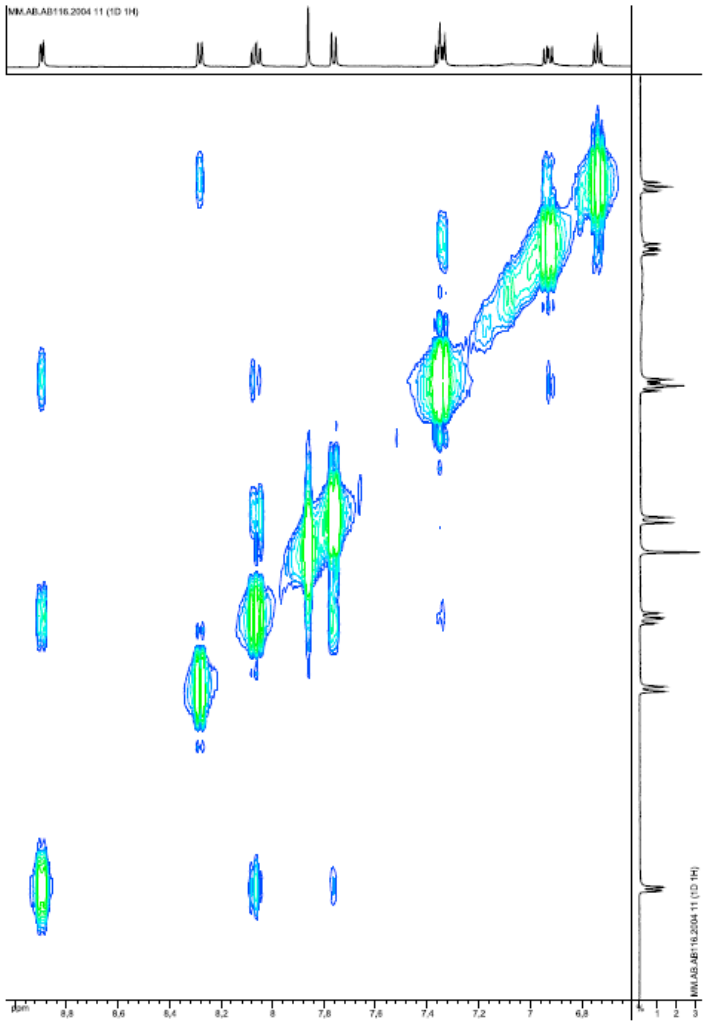

Figure S10. ^{1}H-^{1}H NOESY NMR spectrum recorded for complex **2** in CD_2Cl_2 at 298 K.

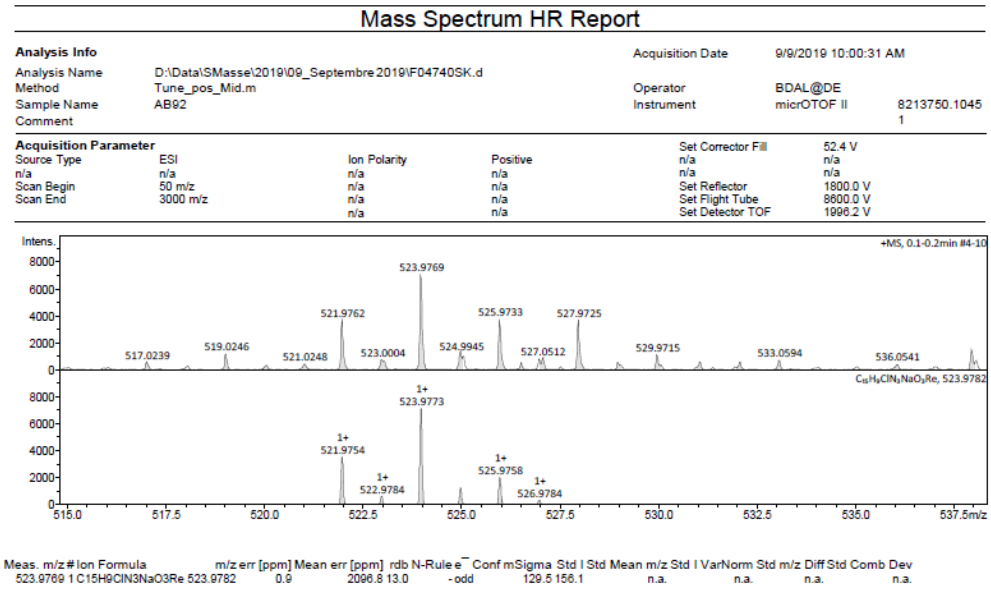

Figure S11. High-resolution ESI-MS spectrum of compound **1**.

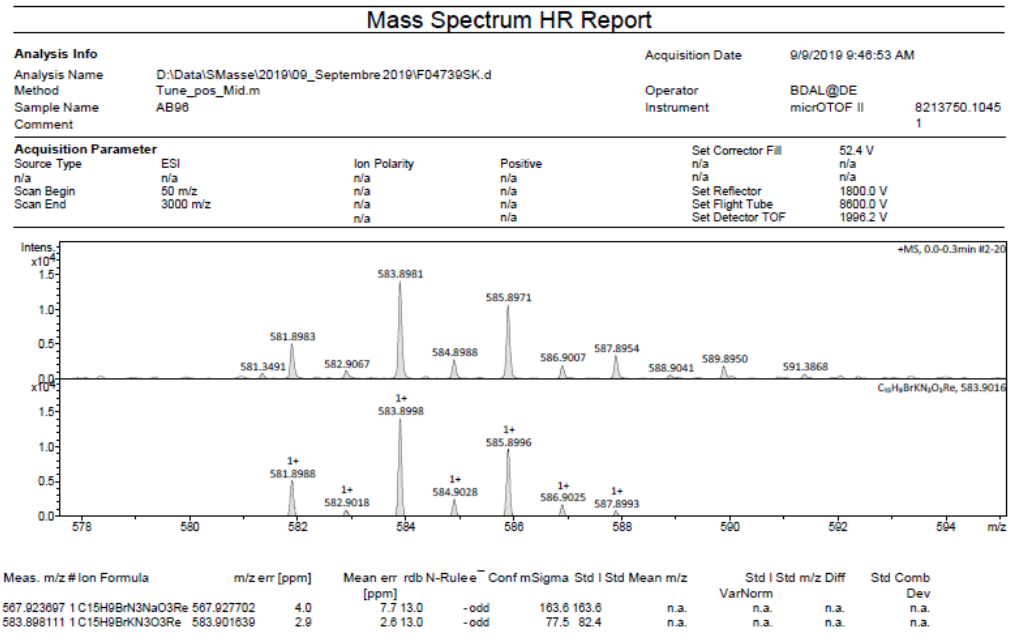

Figure S12. High-resolution ESI-MS spectrum of compound **2**.

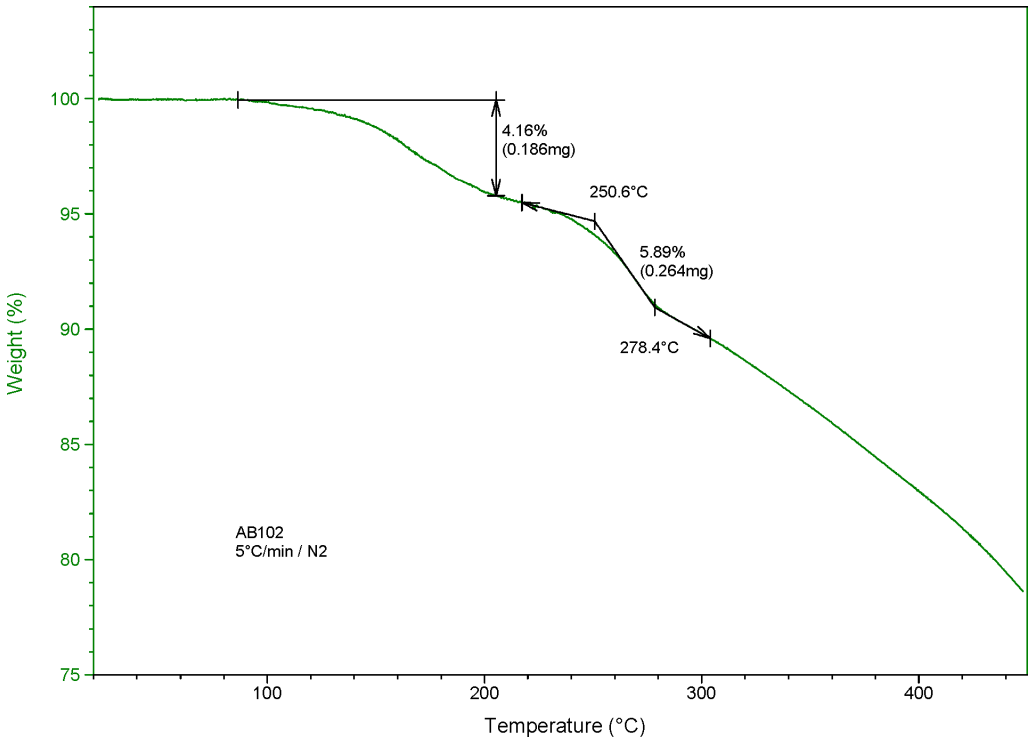

Figure S13. Thermogravimetric analysis recorded for complex **1**.

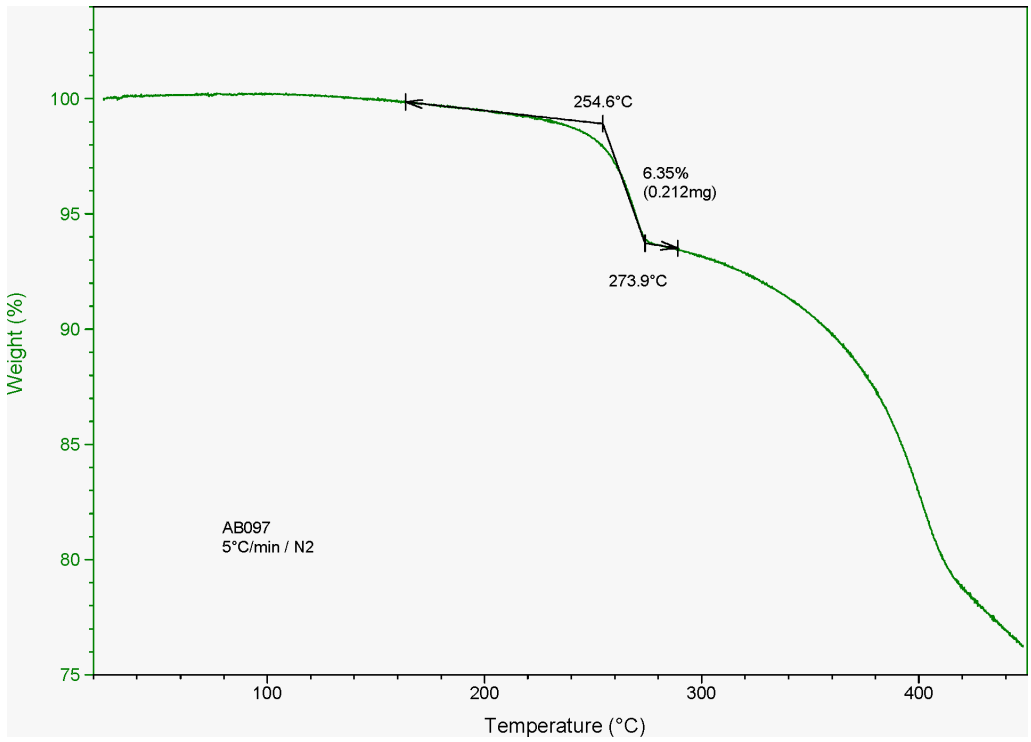

Figure S14. Thermogravimetric analysis recorded for complex **2**.

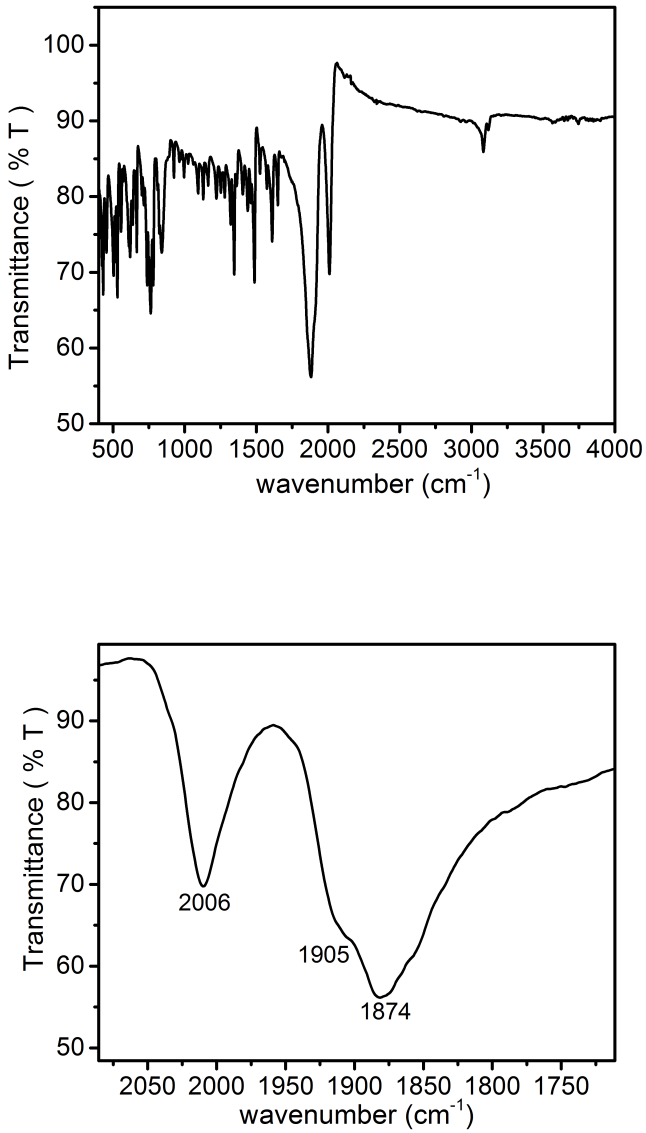

Figure S15. FT-ATR-IR spectra obtained for complex **1** in solid state as neat powder in the region 4000 – 400 cm^{-1} (*top*) and enlarged spectrum in the νC≡O region 2085 – 1711 cm^{-1} (*bottom*).

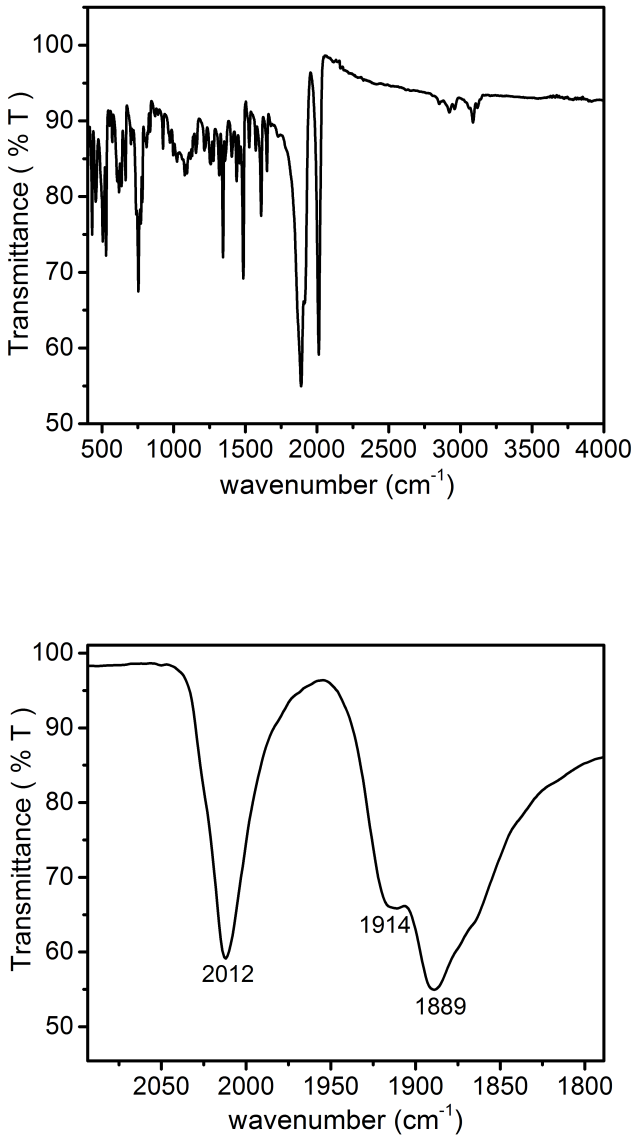

Figure S16. FT-ATR-IR spectra obtained for complex **2** in solid state as neat powder in the region 4000 – 400 cm^{-1} (*top*) and enlarged spectrum in the νC≡O region 2093 – 1788 cm^{-1} (*bottom*).

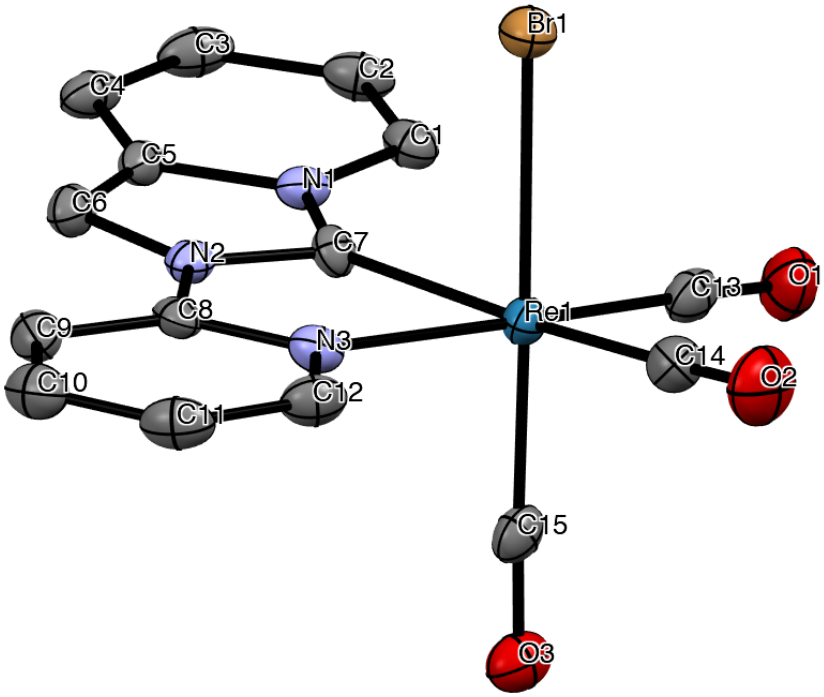

Figure S17. ORTEP diagram of compound **2** with thermal ellipsoids shown at 50% probability level obtained by single-crystal X-ray diffractometric analysis. Hydrogen atoms are omitted for clarity. Selected bond lengths (Å): Re–C(7) = 2.129(4) Å; Re–C(13) = 1.915(5) Å, Re–C(14) = 1.951(5) Å, Re–C(15) = 1.910(5) Å, Re–N(3) = 2.208(4) Å; Re–Br(1) = 2.6199(5) Å.

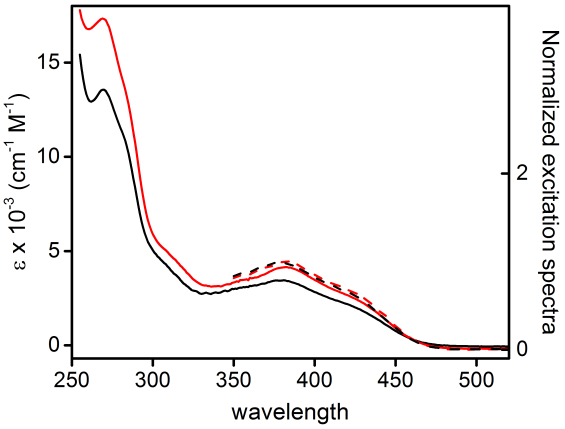

Figure S18. Electronic absorption (solid line) and normalized excitation spectra (dashed line) of complex **1** (black traces) and **2** (red traces) in degassed CH_2Cl_2 solution at a concentration of 2×10^{-5} M at room temperature. Excitation spectra were recorded setting emission at λ_{em} = 660 nm.

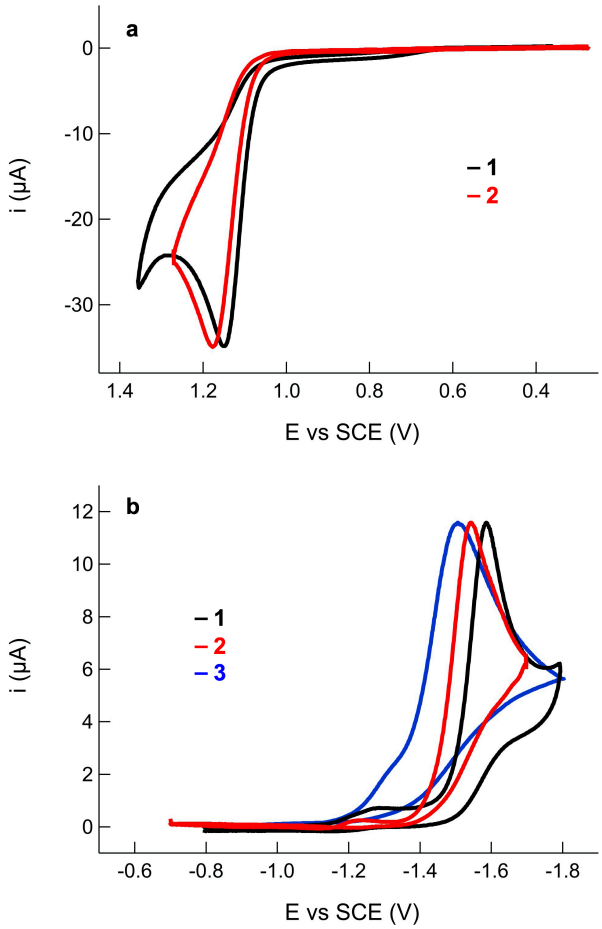

Figure S19. Blank-subtracted CVs recorded for 1 mM of compounds **1** (trace 1), compound **2** (trace 2) and ligand [pyipy]PF_6 (trace 3) in DMF/0.1 M TBAP. Scan rate: 0.1 V s^{-1}. (a) anodic and (b) cathodic processes.

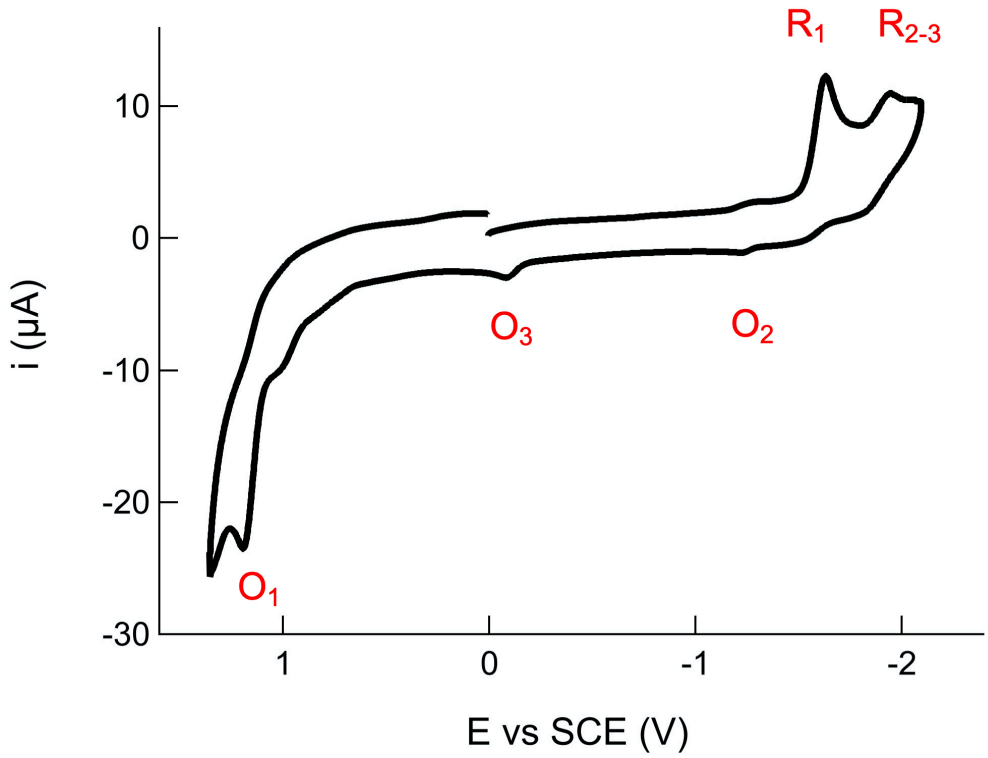

Figure S20. Full range CV of 1 mM **1** in DMF/0.1 M TBAP covering both the reduction and oxidation processes. Scan rate: 0.1 V s^{-1}.

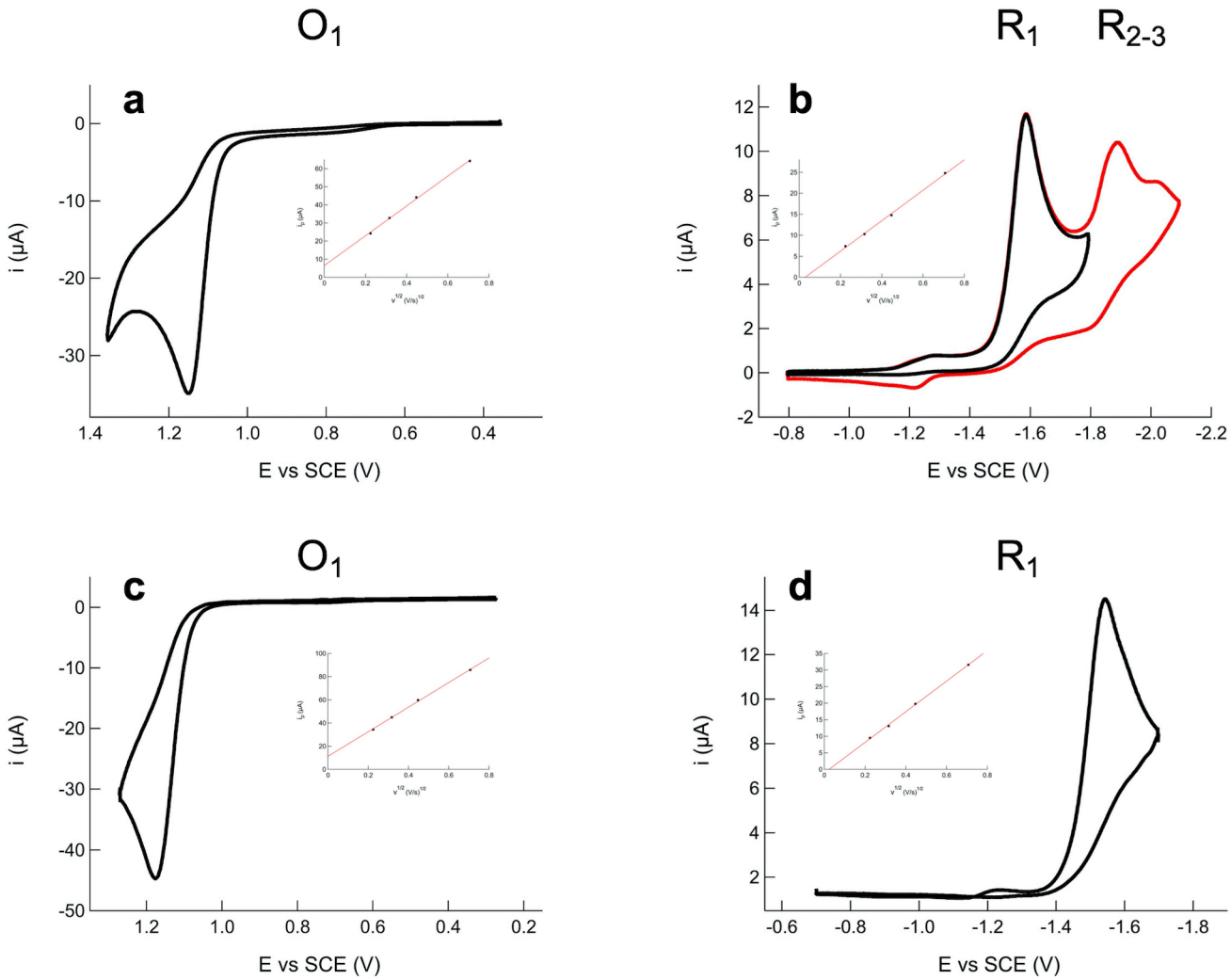

Figure S21. CVs in DMF/0.1 M TBAP showing the oxidation (a) and reduction (b) processes of 1 mM 1, and the oxidation (c) and reduction processes (d) of 1 mM **2**. The insets provide the electrochemical analyses (peak current, i_p, vs the square root of the scan rate, $v^{1/2}$) assessing the diffusion-controlled regime of the redox processes. The redox process for **1** in the negative bias covering also R_2 and R_3 is also shown (red line, b).

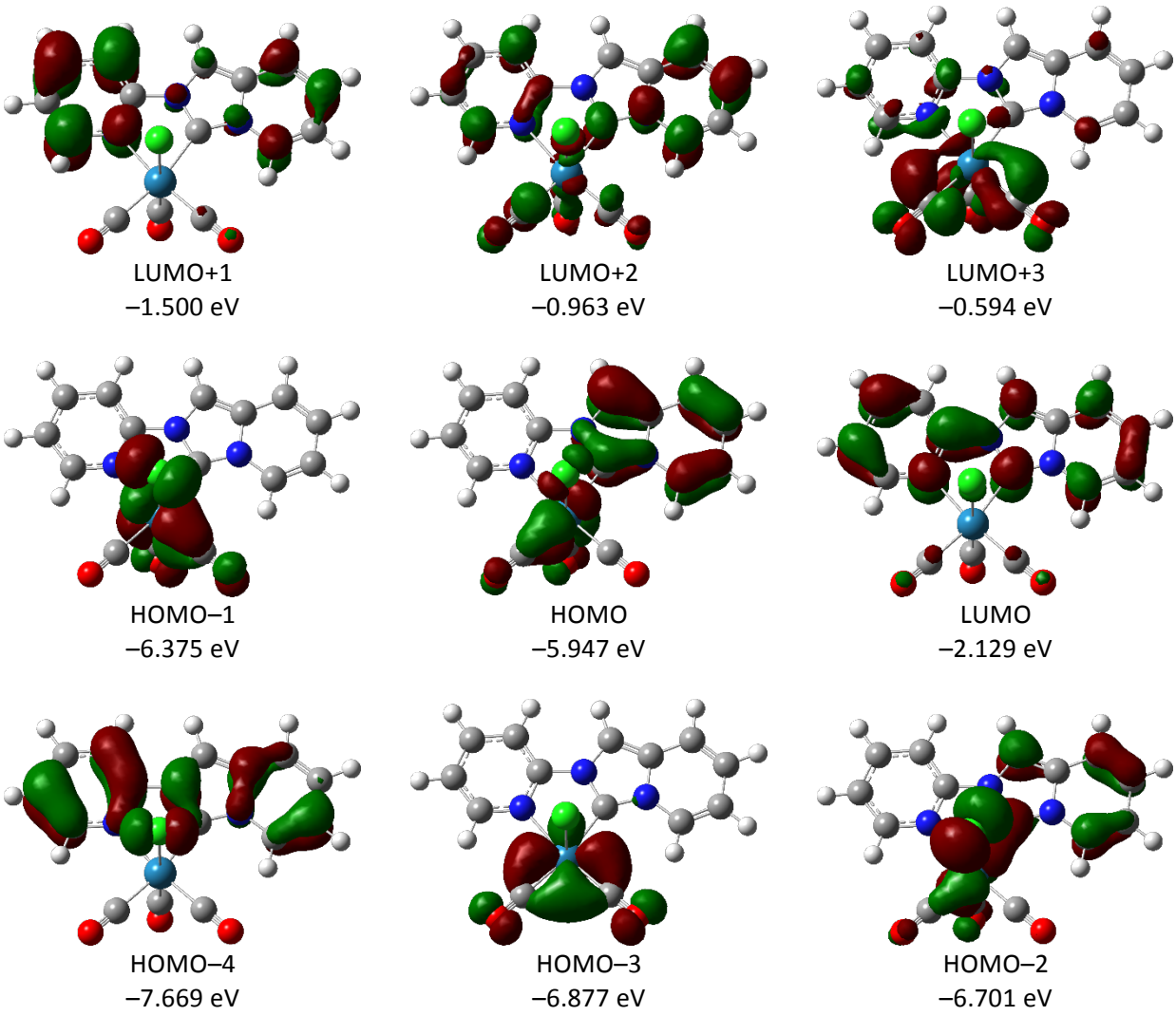

Figure S22. Isodensity surface plots and energies computed for some relevant molecular orbitals of *fac*-[Re(pyipy)$(CO)_3$Cl] (**1**).

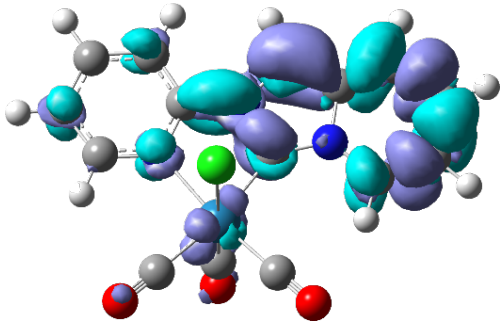

$T_1 \rightarrow S_0$
vertical transition: 1.598 eV; 776 nm
adiabatic transition: 1.982 eV; 626 nm

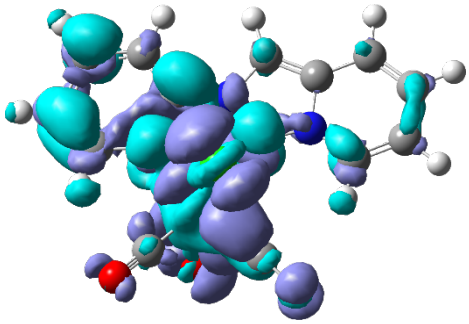

$T_2 \rightarrow S_0$
vertical transition: 2.344 eV; 529 nm
adiabatic transition: 2.831 eV; 438 nm

Figure S23. Electronic density difference maps computed (at the optimized geometry of the corresponding triplet) for the vertical transition $T_1 \rightarrow S_0$ and $T_2 \rightarrow S_0$ of *fac*-[Re(pyipy)(CO)$_3$Cl] (**1**). Energy computed for the corresponding adiabatic transition is also reported. The difference in energy between the T_1 and T_2 minima is 31.210 mE_h (0.849 eV; 6850 cm^{-1}).

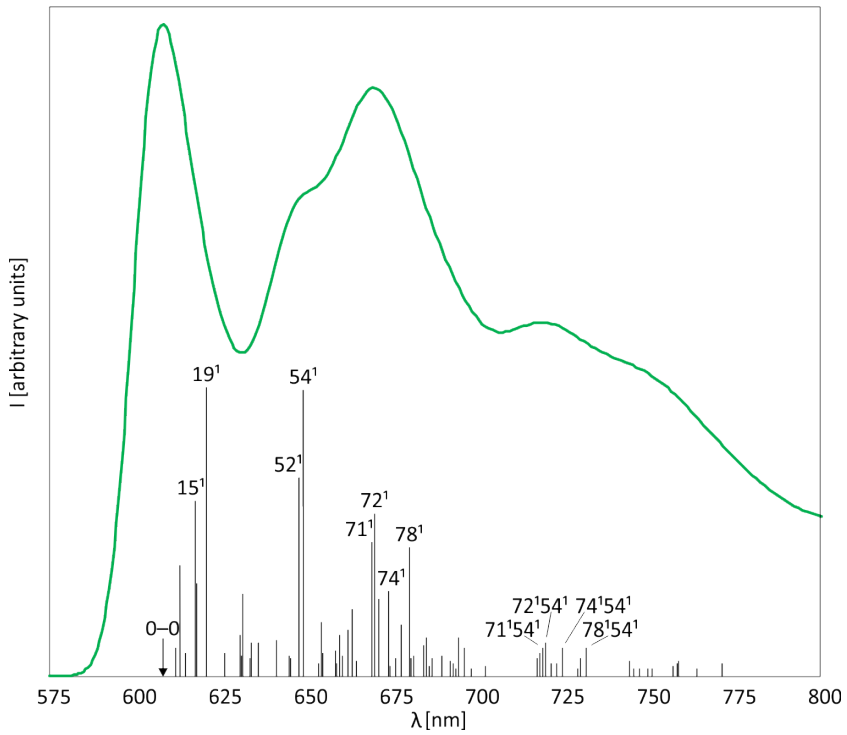

Figure S24. Assignment of the main bands of the computed emission spectrum of the $T_1 \rightarrow S_0$ electronic transition of *fac*-[Re(pyipy)(CO)$_3$Cl] (**1**). The solid line reports the harmonic spectrum calculated within the Franck-Condon approximation (half-width at half-maximum set to 220 cm^{-1}) and the sticks are labelled as ν^x where ν is the ground state normal mode and x its quantum number.

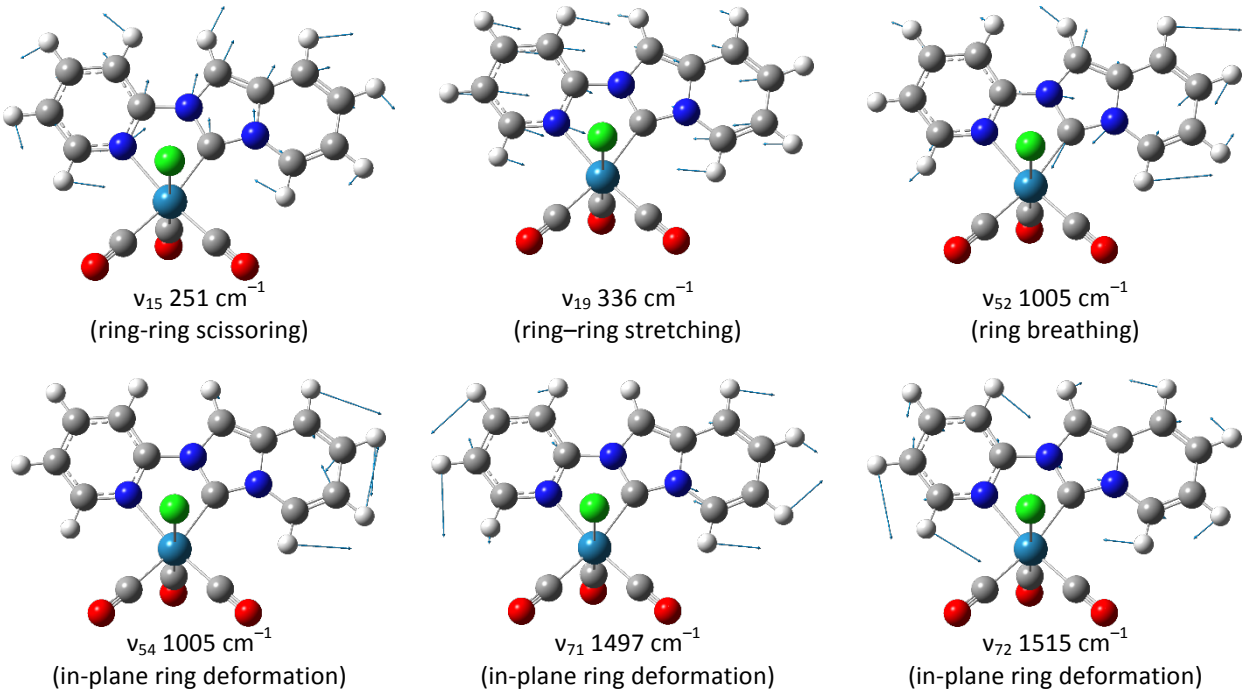

Figure S25. Some relevant normal modes computed for the ground state of *fac*-[Re(pyipy)$(CO)_3$Cl] (**1**).

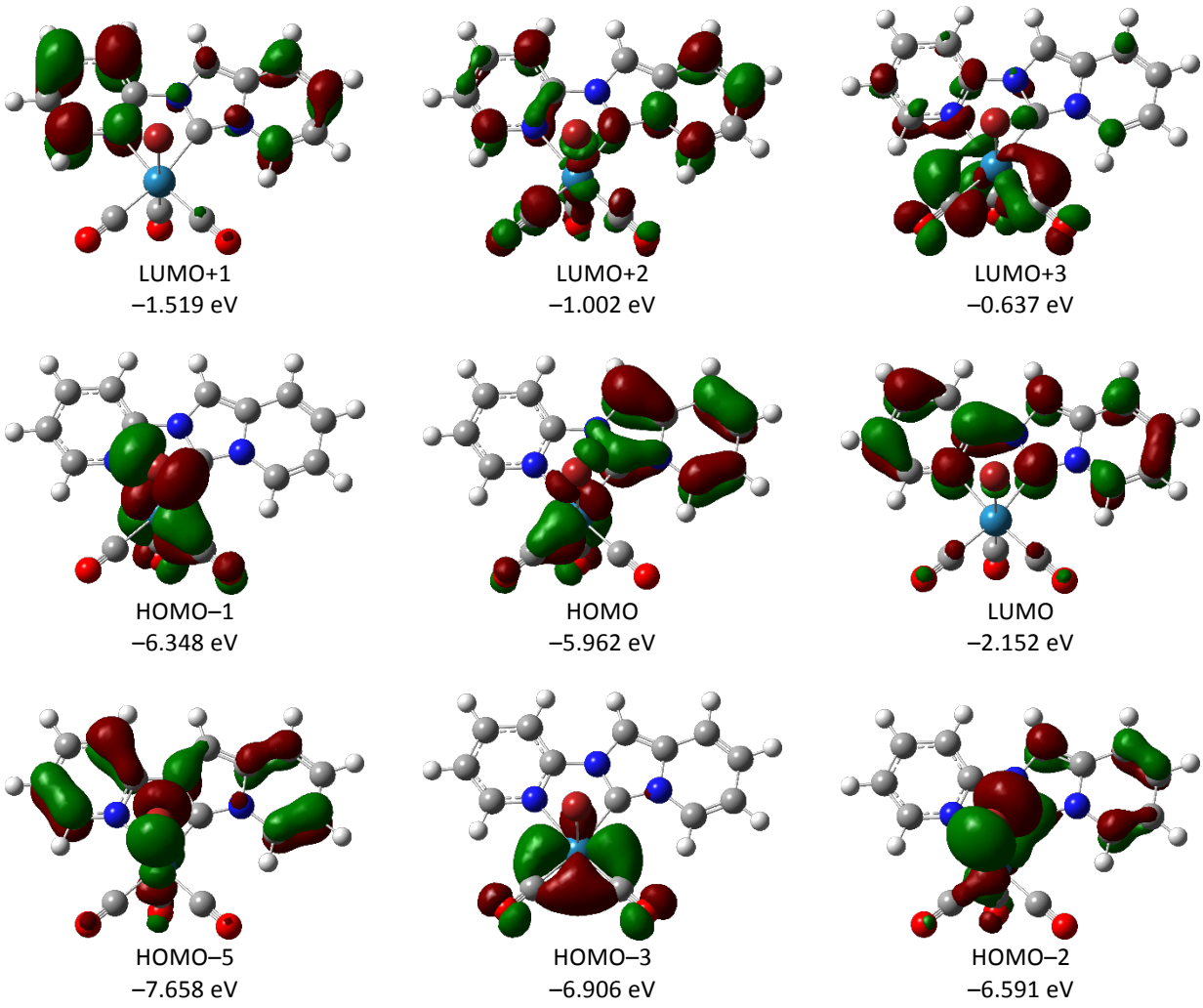

Figure S26. Isodensity surface plots and energies computed for some relevant molecular orbitals of *fac*-[Re(pyipy)$(CO)_3$Br] (**2**).

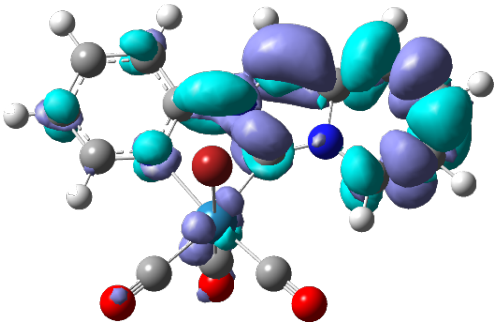

$T_1 \rightarrow S_0$
vertical transition: 1.598 eV; 776 nm
adiabatic transition: 1.979 eV; 626 nm

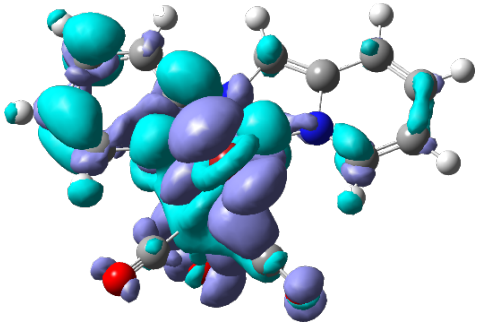

$T_2 \rightarrow S_0$
vertical transition: 2.362 eV; 525 nm
adiabatic transition: 2.825 eV; 439 nm

Figure S27. Electronic density difference maps computed (at the optimized geometry of the corresponding triplet) for the vertical transition $T_1 \rightarrow S_0$ and $T_2 \rightarrow S_0$ of *fac*-[Re(pypi)$(CO)_3$Br] (**2**). Energy computed for the corresponding adiabatic transition is also reported. The difference in energy between the T_1 and T_2 minima is 31.088 mE_h (0.846 eV; 6823 cm^{-1}). Cyan and violet indicates a decrease and increase in electron density, respectively.

Table S1. Crystal data and structure refinement for compound **1**.

Identification code	CCDC 1973530
Empirical formula	C15 H9 Cl N3 O3 Re
Formula weight	500.90
Temperature	120(2) K
Wavelength	0.71073 Å
Crystal system, space group	Triclinic, P -1
Unit cell dimensions	*a* = 6.6594(2) Å α = 89.3060(10)° *b* = 10.8376(4) Å β = 77.6610(10)° *c* = 11.1557(4) Å γ = 72.2660(10)°
Volume	747.94(4) Å^3
Z, Calculated density	2, 2.224 Mg/m^3
Absorption coefficient	8.319 mm^{-1}
F(000)	472
Crystal size	0.200 x 0.150 x 0.120 mm
Theta range for data collection	1.976 to 30.076 deg.
Limiting indices	-9<=*h*<=9, -15<=*k*<=13, -15<=*l*<=15
Reflections collected / unique	54563 / 4399 [R(int) = 0.0367]
Completeness to theta = 25.242	99.9%
Absorption correction	Semi-empirical from equivalents
Max. and min. transmission	0.7460 and 0.6059
Refinement method	Full-matrix least-squares on F^2
Data / restraints / parameters	4399 / 0 / 208
Goodness-of-fit on F^2	1.106
Final R indices [I>2σ(I)]	*R*1 = 0.0152, wR2 = 0.0302
R indices (all data)	*R*1 = 0.0163, wR2 = 0.0305
Extinction coefficient	n/a
Largest diff. peak and hole	1.616 and -0.985 *e* Å^{-3}

Table S2. Geometrical parameters obtained for compound **1** by means of X-ray crystallographic analysis.

Bond lengths [A]

C(1)-C(2)	1.347(3)
C(1)-N(1)	1.396(3)
C(1)-H(1)	0.9500
C(2)-C(3)	1.437(3)
C(2)-H(2)	0.9500
C(3)-C(4)	1.353(3)
C(3)-H(3)	0.9500
C(4)-C(5)	1.425(3)
C(4)-H(4)	0.9500
C(5)-C(6)	1.365(3)
C(5)-N(1)	1.415(3)
C(6)-N(2)	1.387(2)
C(6)-H(6)	0.9500
C(7)-N(1)	1.359(3)
C(7)-N(2)	1.370(3)
C(7)-Re(1)	2.126(2)
C(8)-N(3)	1.342(3)
C(8)-C(9)	1.386(3)
C(8)-N(2)	1.411(3)
C(9)-C(10)	1.384(3)
C(9)-H(9)	0.9500
C(10)-C(11)	1.389(3)
C(10)-H(10)	0.9500
C(11)-C(12)	1.378(3)
C(11)-H(11)	0.9500
C(12)-N(3)	1.358(3)
C(12)-H(12)	0.9500
C(13)-O(1)	1.156(3)
C(13)-Re(1)	1.913(2)
C(14)-O(2)	1.145(3)
C(14)-Re(1)	1.957(2)
C(15)-O(3)	1.147(3)
C(15)-Re(1)	1.914(2)
N(3)-Re(1)	2.2085(17)
Cl(1)-Re(1)	2.5049(5)

Bond angles [°]

C(2)-C(1)-N(1)	119.1(2)
C(2)-C(1)-H(1)	120.5
N(1)-C(1)-H(1)	120.5
C(1)-C(2)-C(3)	121.3(2)
C(1)-C(2)-H(2)	119.4
C(3)-C(2)-H(2)	119.4
C(4)-C(3)-C(2)	120.5(2)
C(4)-C(3)-H(3)	119.8
C(2)-C(3)-H(3)	119.8
C(3)-C(4)-C(5)	119.3(2)
C(3)-C(4)-H(4)	120.3
C(5)-C(4)-H(4)	120.3
C(6)-C(5)-N(1)	106.30(17)
C(6)-C(5)-C(4)	134.8(2)
N(1)-C(5)-C(4)	118.85(19)
C(5)-C(6)-N(2)	105.53(17)

C(5)-C(6)-H(6)	127.2
N(2)-C(6)-H(6)	127.2
N(1)-C(7)-N(2)	102.88(16)
N(1)-C(7)-Re(1)	140.64(15)
N(2)-C(7)-Re(1)	116.36(14)
N(3)-C(8)-C(9)	124.18(19)
N(3)-C(8)-N(2)	113.63(17)
C(9)-C(8)-N(2)	122.18(18)
C(10)-C(9)-C(8)	117.66(19)
C(10)-C(9)-H(9)	121.2
C(8)-C(9)-H(9)	121.2
C(9)-C(10)-C(11)	119.5(2)
C(9)-C(10)-H(10)	120.2
C(11)-C(10)-H(10)	120.2
C(12)-C(11)-C(10)	118.9(2)
C(12)-C(11)-H(11)	120.5
C(10)-C(11)-H(11)	120.5
N(3)-C(12)-C(11)	122.7(2)
N(3)-C(12)-H(12)	118.6
C(11)-C(12)-H(12)	118.6
O(1)-C(13)-Re(1)	176.2(2)
O(2)-C(14)-Re(1)	177.1(2)
O(3)-C(15)-Re(1)	178.6(2)
C(7)-N(1)-C(1)	127.11(18)
C(7)-N(1)-C(5)	111.86(17)
C(1)-N(1)-C(5)	120.99(17)
C(7)-N(2)-C(6)	113.41(17)
C(7)-N(2)-C(8)	118.68(17)
C(6)-N(2)-C(8)	127.90(17)
C(8)-N(3)-C(12)	116.99(18)
C(8)-N(3)-Re(1)	117.26(13)
C(12)-N(3)-Re(1)	125.64(14)
C(13)-Re(1)-C(15)	87.28(9)
C(13)-Re(1)-C(14)	89.70(9)
C(15)-Re(1)-C(14)	91.94(9)
C(13)-Re(1)-C(7)	100.48(9)
C(15)-Re(1)-C(7)	94.99(8)
C(14)-Re(1)-C(7)	167.92(9)
C(13)-Re(1)-N(3)	173.71(8)
C(15)-Re(1)-N(3)	90.34(8)
C(14)-Re(1)-N(3)	96.20(8)
C(7)-Re(1)-N(3)	73.92(7)
C(13)-Re(1)-Cl(1)	95.95(7)
C(15)-Re(1)-Cl(1)	176.71(7)
C(14)-Re(1)-Cl(1)	87.46(7)
C(7)-Re(1)-Cl(1)	85.05(5)
N(3)-Re(1)-Cl(1)	86.51(5)

Table S3. Crystal data and structure refinement for compound **2**.

Identification code	CCDC 1980932
Empirical formula	C15 H9 Br N3 O3 Re
Formula weight	545.36
Temperature	120(2) K
Wavelength	0.71073 Å
Crystal system, space group	Triclinic, P -1
Unit cell dimensions	*a* = 6.7338(3) Å α = 88.7910(10)° *b* = 10.8986(4) Å β = 76.4800(10)° *c* = 11.3120(5) Å γ = 72.1440(10)°
Volume	767.14(6) Å^3
Z, Calculated density	2, 2.361 Mg/m^3
Absorption coefficient	10.542 mm^{-1}
F(000)	508
Crystal size	0.180 x 0.150 x 0.120 mm
Theta range for data collection	1.966 to 29.168 deg.
Limiting indices	-9<=h<=9, -14<=k<=14, -15<=l<=15
Reflections collected / unique	54752 / 4137 [R(int) = 0.0597]
Completeness to theta = 25.242	100.0 %
Absorption correction	Semi-empirical from equivalents
Max. and min. transmission	0.7458 and 0.5741
Refinement method	Full-matrix least-squares on F^2
Data / restraints / parameters	4137 / 0 / 208
Goodness-of-fit on F^2	1.109
Final R indices [I>2σ(I)]	*R*1 = 0.0295, w*R*2 = 0.0621
R indices (all data)	*R*1 = 0.0342, w*R*2 = 0.0649
Extinction coefficient	n/a
Largest diff. peak and hole	3.362 and -1.941 *e* Å^{-3}

Table S4. Geometrical parameters obtained for compound **2** by means of X-ray crystallographic analysis.

Bond lengths [A]	
C(1)-C(2)	1.347(7)
C(1)-N(1)	1.396(6)
C(1)-H(1)	0.9500
C(2)-C(3)	1.440(8)
C(2)-H(2)	0.9500
C(3)-C(4)	1.339(8)
C(3)-H(3)	0.9500
C(4)-C(5)	1.428(7)
C(4)-H(4)	0.9500
C(5)-C(6)	1.359(7)
C(5)-N(1)	1.416(6)
C(6)-N(2)	1.384(6)
C(6)-H(6)	0.9500
C(7)-N(1)	1.349(6)
C(7)-N(2)	1.374(6)
C(7)-Re(1)	2.129(4)
C(8)-N(3)	1.344(6)
C(8)-C(9)	1.381(7)
C(8)-N(2)	1.411(6)
C(9)-C(10)	1.385(7)
C(9)-H(9)	0.9500
C(10)-C(11)	1.382(8)
C(10)-H(10)	0.9500
C(11)-C(12)	1.380(8)
C(11)-H(11)	0.9500
C(12)-N(3)	1.355(6)
C(12)-H(12)	0.9500
C(13)-O(1)	1.154(6)
C(13)-Re(1)	1.915(5)
C(14)-O(2)	1.150(6)
C(14)-Re(1)	1.951(5)
C(15)-O(3)	1.146(6)
C(15)-Re(1)	1.910(5)
N(3)-Re(1)	2.208(4)
Br(1)-Re(1)	2.6199(5)

Bond angles [°]	
C(2)-C(1)-N(1)	118.6(5)
C(2)-C(1)-H(1)	120.7
N(1)-C(1)-H(1)	120.7
C(1)-C(2)-C(3)	121.2(5)
C(1)-C(2)-H(2)	119.4
C(3)-C(2)-H(2)	119.4
C(4)-C(3)-C(2)	121.0(5)

C(4)-C(3)-H(3)	119.5
C(2)-C(3)-H(3)	119.5
C(3)-C(4)-C(5)	119.3(5)
C(3)-C(4)-H(4)	120.4
C(5)-C(4)-H(4)	120.4
C(6)-C(5)-N(1)	106.2(4)
C(6)-C(5)-C(4)	135.2(5)
N(1)-C(5)-C(4)	118.6(5)
C(5)-C(6)-N(2)	106.0(4)
C(5)-C(6)-H(6)	127.0
N(2)-C(6)-H(6)	127.0
N(1)-C(7)-N(2)	103.3(4)
N(1)-C(7)-Re(1)	140.7(3)
N(2)-C(7)-Re(1)	115.8(3)
N(3)-C(8)-C(9)	124.7(4)
N(3)-C(8)-N(2)	113.2(4)
C(9)-C(8)-N(2)	122.1(4)
C(8)-C(9)-C(10)	117.5(5)
C(8)-C(9)-H(9)	121.2
C(10)-C(9)-H(9)	121.2
C(11)-C(10)-C(9)	119.4(5)
C(11)-C(10)-H(10)	120.3
C(9)-C(10)-H(10)	120.3
C(12)-C(11)-C(10)	119.1(5)
C(12)-C(11)-H(11)	120.4
C(10)-C(11)-H(11)	120.4
N(3)-C(12)-C(11)	122.8(5)
N(3)-C(12)-H(12)	118.6
C(11)-C(12)-H(12)	118.6
O(1)-C(13)-Re(1)	177.5(5)
O(2)-C(14)-Re(1)	177.8(5)
O(3)-C(15)-Re(1)	177.9(5)
C(7)-N(1)-C(1)	126.8(4)
C(7)-N(1)-C(5)	111.8(4)
C(1)-N(1)-C(5)	121.4(4)
C(7)-N(2)-C(6)	112.7(4)
C(7)-N(2)-C(8)	119.3(4)
C(6)-N(2)-C(8)	128.0(4)
C(8)-N(3)-C(12)	116.4(4)
C(8)-N(3)-Re(1)	117.5(3)
C(12)-N(3)-Re(1)	126.0(3)
C(15)-Re(1)-C(13)	87.4(2)
C(15)-Re(1)-C(14)	91.9(2)
C(13)-Re(1)-C(14)	89.8(2)
C(15)-Re(1)-C(7)	95.33(19)
C(13)-Re(1)-C(7)	100.16(19)
C(14)-Re(1)-C(7)	167.9(2)
C(15)-Re(1)-N(3)	91.48(18)
C(13)-Re(1)-N(3)	174.05(18)
C(14)-Re(1)-N(3)	96.07(19)
C(7)-Re(1)-N(3)	74.11(16)

C(15)-Re(1)-Br(1)	177.35(16)
C(13)-Re(1)-Br(1)	95.01(15)
C(14)-Re(1)-Br(1)	87.03(15)
C(7)-Re(1)-Br(1)	85.31(12)
N(3)-Re(1)-Br(1)	86.22(10)

Table S5. Properties of some of the more intense electronic transitions computed for *fac*-[Re(pyipy)$(CO)_3$Cl] (**1**). In the electronic density difference maps (EDDMs), cyan and violet indicates a decrease and increase in electron density, respectively.

S_n	E [eV]	λ [nm]	f			EDDM
1	2.982	416	0.0531	HOMO→LUMO	93%	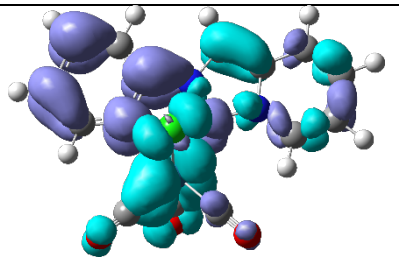 $S_0 \rightarrow S_1$
2	3.325	373	0.0641	HOMO–1→LUMO	92%	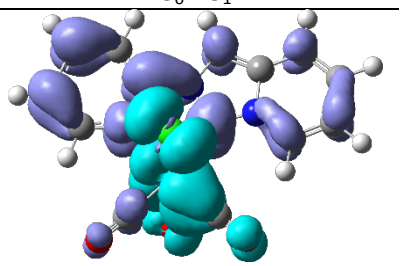 $S_0 \rightarrow S_2$
14	4.679	265	0.1285	HOMO–4→LUMO HOMO–2→LUMO+2	55% 9%	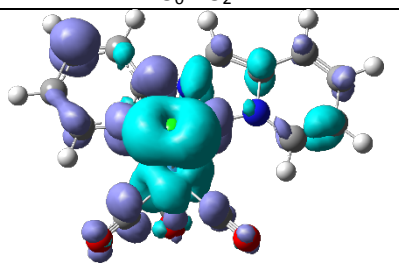 $S_0 \rightarrow S_{14}$
17	4.867	255	0.1033	HOMO–2→LUMO+2	72%	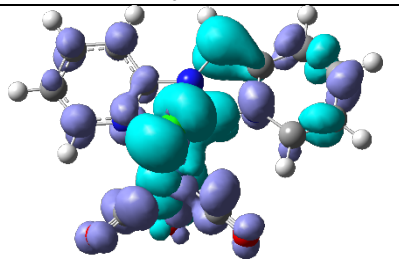 $S_0 \rightarrow S_{17}$
21	5.138	241	0.1813	HOMO–2→LUMO+3 HOMO–6→LUMO HOMO→LUMO+5	34% 13% 9%	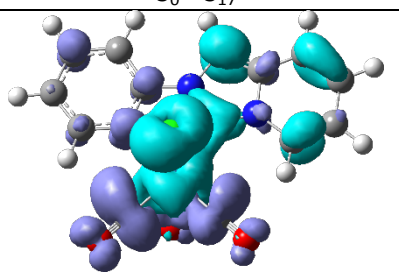 $S_0 \rightarrow S_{21}$

Table S6. Properties of some of the more intense electronic transitions computed for *fac*-[Re(pyipy)(CO)$_3$Br] (**2**). In the electronic density difference maps (EDDMs), cyan and violet indicates a decrease and increase in electron density, respectively.

S_n	E [eV]	λ [nm]	f			EDDM
1	2.975	417	0.0511	HOMO→LUMO	92%	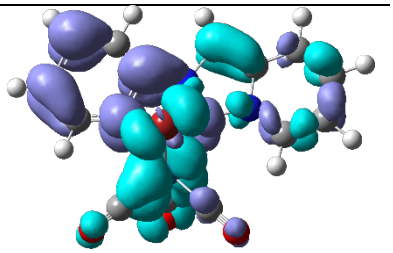 $S_0 \rightarrow S_1$
2	3.278	378	0.0524	HOMO–1→LUMO	92%	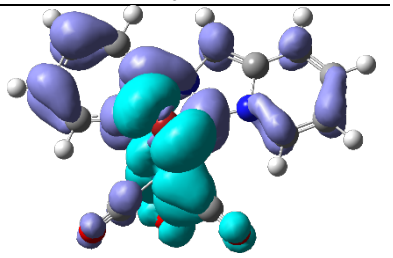 $S_0 \rightarrow S_2$
15	4.616	269	0.0916	HOMO–5→LUMO HOMO–1→LUMO+2	71% 13%	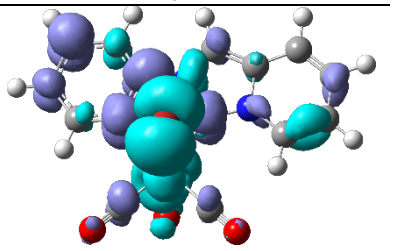 $S_0 \rightarrow S_{15}$
18	4.800	258	0.0901	HOMO–6→LUMO HOMO→LUMO+5	73% 10%	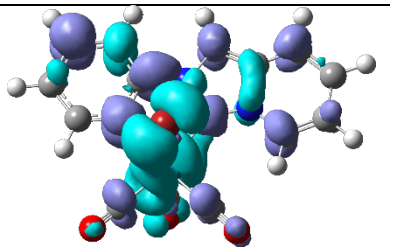 $S_0 \rightarrow S_{18}$